

Characterizing the Effect of Capillary Heterogeneity on Multiphase Flow Pulsation in an Intermediate-Scale Beadpack Experiment using Time Series Clustering and Frequency Analysis

Hailun Ni¹, T.A. Meckel¹

¹Bureau of Economic Geology, Jackson School of Geosciences, The University of Texas at Austin, Austin, USA.

Corresponding author: Hailun Ni (hailun.ni@beg.utexas.edu)

Key Points:

- Conducted a low-rate buoyancy-driven drainage experiment in a dm-scale beadpack and simulations to study nonwetting phase pulsation
- Flow pulsation can cause nonwetting phase fluids such as CO₂ to breach the capillary barriers before bypassing them
- Modified invasion percolation probabilistic simulations can satisfactorily match dynamic experimental fluid flow results

This article has been accepted for publication and undergone full peer review but has not been through the copyediting, typesetting, pagination and proofreading process, which may lead to differences between this version and the Version of Record. Please cite this article as doi: 10.1029/2021WR030876.

Abstract

An intermediate-scale beadpack drainage experiment was conducted to investigate how simple layered lamination heterogeneity affects CO₂ flow. Two simple layers of capillary barriers are manually packed in the tank and slow drainage was carried out using analog fluids to mimic the capillary- and gravity-dominated CO₂ upward migration process in deep saline aquifers. Nonwetting phase saturation time series clustering analysis and frequency analysis have been conducted on the experimental data. Additionally, modified invasion percolation numerical simulations were done on a digital model of the beadpack to compare to experimental results. Results show that capillary barriers can lead to strong pulsation behavior, which in turn can cause unexpected early breaching through other barriers. The inlet pressure is found to be able to respond to saturation changes in far regions of the domain, indicating that the wetting phase can transmit pressure changes from the other phase. Although static simulations were not able to capture all the dynamic behavior observed in the experiment, Monte Carlo composite simulation results combining many different realizations can better illustrate how the nonwetting phase will behave in the heterogeneous domain. Our results suggest the need for CO₂ storage site selection with preference given to aquifers with more capillary barriers with finer grain sizes to avoid flow pulsation and to retard plume upward migration.

1 Introduction

CO₂ geologic storage is an essential part of climate change solutions. Not only can it allow our fossil-fuel dominated society to achieve carbon neutrality while transitioning toward more renewables, but when combined with biomass energy or direct air capture, CO₂ geologic storage is a key component of negative carbon pathways (IPCC, 2005, 2014; Rogelj et al., 2018; Wilcox et al., 2021). One major target for CO₂ geologic storage is deep saline aquifers due to their large storage capacity and widespread availability (IPCC, 2005). However, in the sedimentary basins where these saline aquifers are located, the rock formations all have natural geologic fabrics (depositional textures at cm-to-m scales) that can be highly heterogeneous (Murphy et al., 1984; Rubin & Carter, 1987). Even small-scale heterogeneities (cm-scale) can significantly affect CO₂ migration and trapping (Corbett et al., 1992; Huang et al., 1995; Jackson & Krevor, 2020; Kortekaas, 1985; Krevor et al., 2011; Meckel et al., 2015; Saadatpoor et al., 2010; Trevisan et al., 2017a). Therefore, in order to accurately estimate CO₂ plume size and trapping capacity, it is necessary to conduct accurate simulation studies before project commencement.

Currently in the CO₂ storage field, two kinds of common fluid flow simulation methods exist, the Darcy-flow simulation method and the modified invasion percolation (MIP) simulation method. In CO₂ geologic storage, the Darcy-flow simulation method is necessary during injection at locations close to the injection well because the viscous forces are strong. However, at locations away from the injection well or when injection has stopped, the flow rates are low enough that viscous forces are negligible and CO₂ migration is dominated by capillary and gravity forces (Jackson & Krevor, 2020). For this flow regime, by assuming infinitesimal flow rates and ignoring viscous forces, the MIP simulation method can rapidly predict plume migration (Celia et al., 2015). Although Darcy-flow simulators should produce similar results if capillary heterogeneity is properly included, IP-based simulators take fewer inputs, can run faster, and can handle finer grids (Ni et al., 2021). In order to ensure that the simulation results are reliable and correct, experiments need to be done to validate simulation results and improve simulator capabilities.

CO₂ flow under strongly capillary- and gravity-dominated conditions are especially susceptible to the influence of cm-to-m scale geologic heterogeneity (Meckel et al., 2015; Trevisan et al., 2017a). However, pore-scale and core-scale experiments such as micromodel, microCT, and coreflooding experiments lack the larger domain size necessary to capture heterogeneity at the cm-to-m scale. The intermediate tank-scale experiments on the other hand, while capable of capturing heterogeneity at the larger scale, can also replicate the strong gravity forces present due to its larger domain size. Furthermore, tank-scale experiments have the advantage of allowing easy engineering of different types and degrees of heterogeneous domains, making these kinds of experiments ideal for studying the effect of capillary heterogeneity on CO₂ migration and trapping.

In prior publications, tank-scale experiments are often used to help us better understand how CO₂ would behave in heterogeneous geologic domains. Trevisan et al. (2017b) conducted large sand tank experiments and have found that CO₂ plume migrates upward much more slowly in heterogeneous domains than in homogeneous domains. Later Trevisan et al. (2017c) carried out MIP simulations (PermediaTM) and have found satisfactory matching between the tank-scale experimental results and the MIP simulation results. More recently, Krishnamurthy (2020) conducted a series of tank-scale beadpack experiments with different grain size contrasts between the matrix and the laminae and have concluded that an increasing degree of heterogeneity of the domain increases post-drainage CO₂ saturation. This is also consistent with MIP simulation results.

While previous tank-scale experimental studies have focused on how heterogeneity affects the eventual post-drainage and post-imbibition CO₂ distribution and saturation, the actual dynamics of how CO₂ migrates through a heterogeneous domain at low flow rates is also important to understand. From the beadpack experiments, Krishnamurthy (2020) has found that when the degree of heterogeneity is low, nonwetting phase (NWP) under buoyancy is transported in thin tendril-like fingers. Whereas when the degree of heterogeneity is high, NWP flows upward under buoyancy until it hits a capillary barrier and accumulates in a pool underneath. Only when the column height of the pool is large enough can the NWP break through and continue its upward migration (Glass et al., 2000; Krishnamurthy, 2020).

Much past vertical beadpack work has been done on NWP flow dynamics in fingers in homogeneous domains (Birovljev et al., 1995; Islam et al., 2014; Luo et al., 2004; Meakin et al., 2000; Stöhr & Khalili, 2006; Wagner et al., 1997) However, less work exists that studies the NWP flow dynamics in pools in heterogeneous domains (Krishnamurthy, 2020). To the best of our knowledge, Glass et al. (2000) conducted perhaps the only relevant tank-scale slow drainage experimental study focuses on the combined dynamic effect of both types of NWP drainage (fingers and pools) together in a single experiment. The authors observed how the NWP migrates through flowpaths consist of a series of fingers and pools under gravity and they also observed clear pulsation in these flowpaths. Additionally, the authors have advocated for Monte Carlo simulation using MIP methods to better predict low-rate NWP migration under gravity in heterogeneous domains.

Therefore, in this study, we conduct an intermediate-scale drainage beadpack experiment similar to what Glass et al. (2000) did, but with much simpler layered heterogeneity in order to make detailed observations on how capillary barriers affect CO₂ flow dynamics. We also compare our experimental results to MIP numerical simulation results to see how the NWP saturation results differ.

2 Material and methods

An immiscible two-phase drainage experiment with analog fluids representative of deep subsurface conditions (see below) is conducted in a tank filled with glass beads. The size of the tank is 0.6 m by 0.6 m by 0.02 m. Experiments are conducted at atmospheric conditions (pressure at 1 atm and room temperature). The experiment models strongly water-wet conditions, which are typical for quartz-rich saline aquifers (Iglauer et al., 2015). The light transmission visualization method is used to compute NWP saturation. For more information on experimental material and methods, refer to Krishnamurthy et al. (2019) and Krishnamurthy (2020).

2.1 Material

The analog fluid pair is chosen so that their properties are similar to that of the CO₂/water fluid pair at reservoir conditions for a typical CO₂ storage project injecting at around 1km deep as shown in Table 1. The NWP fluid used is heptane dyed with Oil Red O at 40 mg/L concentration and the wetting phase (WP) fluid is a 50%/50% weight mixture of glycerol and deionized water (Krishnamurthy et al., 2019; Krishnamurthy, 2020).

Table 1. Analog fluid properties compared to actual CO₂/brine fluid properties in CO₂ geologic storage (Iglauer, 2018; Krishnamurthy et al., 2019; Krishnamurthy, 2020; Nordbotten et al., 2005).

Fluid	Density (kg/m ³)	Viscosity (mPa·s)	Density ratio (NWP/WP)	Viscosity ratio (NWP/WP)	Interfacial tension (mN/m)
Heptane	684	0.41	0.61	0.066	36
Glycerol/water	1115.4	6.25			
Supercritical CO ₂	714	0.0577	0.58-0.71	0.037-0.073	38.7
Brine	1012-1230	0.795-1.58			

Two types of glass beads are used in the experiment, a coarse type (P337) for the matrix and a fine type (P230) for the capillary barrier (Krishnamurthy et al., 2019; Krishnamurthy, 2020). Much finer glass beads are used to pack the bottom and the sides of the tank to prevent the NWP fluid from unintentionally leaving the domain. The properties of the glass beads are shown in Table 2.

Table 2. Glass bead properties (Krishnamurthy et al., 2019; Krishnamurthy, 2020).

Glass bead type	U.S. sieve size	Mean diameter (mm)	Diameter standard deviation (mm)	Entry pressure (Pa)
Coarse (P337)	20-30	0.689	0.086	216
Fine (P230)	30-40	0.457	0.06	293

Packing of the glass beads into the tank is done manually. The domain consists of a homogeneous coarse-grain matrix with two fine-grain capillary barrier layers going through it. The thickness of the barrier layers is between 1 to 2 cm. Because the grains tend to roll down the slope during packing, barrier layers at the bottom of the slope tend to be slightly thicker than at the top. The exact configuration of the layered heterogeneity can be found in Figure 1.

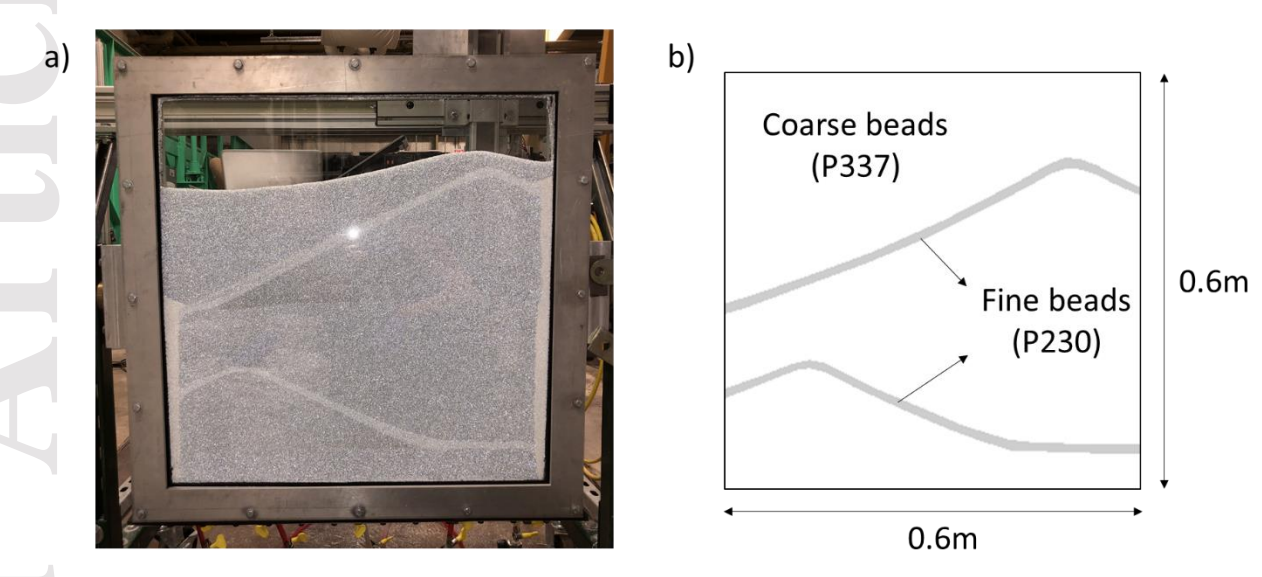


Figure 1. a) Picture of the tank during packing. b) Binary domain used for simulation. The fine beads on the side are not included for simulation because the experimental NWP flow paths never reach the sides. White: matrix; gray: laminae or capillary barrier.

2.2 Experimental procedure

After the tank is packed, it is flooded with gaseous CO₂ at atmospheric conditions for 48 hours at a flow rate of 5 L/min. This is done to displace the air in the pore space with water soluble CO₂ to prevent air bubbles from been trapped in the beadpack. Next, the tank is wheeled into the darkroom in front of the camera. The dry (air-saturated beadpack) reference image is taken. After that, the tank is filled with the WP fluid. An additional 1 pore volume of WP is injected to replace the CO₂-saturated WP in the tank with fresh WP. Then a wet (WP-saturated beadpack) reference image is taken. Now the tank is ready for the flow experiment (Krishnamurthy et al., 2019; Krishnamurthy, 2020).

The flow experiment has a single drainage stage. There are five inlets at the bottom of the tank and a single outlet at the top of the tank. During drainage, NWP is injected through the middle bottom inlet using a peristaltic pump (Masterflex, Cole Parmer) at a low flow rate of 0.2 mL/min for 21 hours. The capillary number $(\nu\mu/\sigma)$ for this experiment is 3.0×10^{-6} (based on NWP injection rate/inlet area), which is similar to other low-rate drainage sand tank experiments (Krishnamurthy, 2020; Trevisan et al., 2017b). This is higher than the field-scale capillary number value range when away from the injection well and viscous forces are no longer significant $(10^{-9}-10^{-8})$ but still within the strongly capillary-dominated flow regime (Jackson & Krevor, 2020; Ni et al., 2021; Ni & Benson, 2020).

2.3 Data acquisition

The conventional light transmission visualization method is used to compute pixel-wise NWP saturation (Bob et al., 2008; Krishnamurthy et al., 2019; Krishnamurthy, 2020; Niemet & Selker, 2001; Tidwell & Glass, 1994). The equations and input parameters used can be found in Supporting Information. During the flow experiment, the tank is illuminated by an LED back panel, and images are acquired with a high-definition monochrome camera. A filter is installed on the camera lens to maximize light passage in the bandwidth of 500 nm to 530 nm, which coincides with the absorbance peak of the dyed heptane. The camera aperture used is F2.8 and the exposure time is 0.3 sec. The size of the square tank image is 2316 by 2316 pixels, and the image pixel dimensions are 0.0252 cm by 0.0252 cm. A total of 2364 images are recorded for the drainage experiment, or one image every 30 seconds.

To compute the overall porosity of the beadpack, multiple images are taken during the WP filling process so that an average porosity value can be obtained from volume calculation using the exact tank internal dimensions listed in Table S1. The resulting average porosity value is 0.399 for this experiment. With this porosity value, we can obtain the pore volume of the tank, and furthermore the NWP volume retained in different parts of the domain.

A pressure transducer is present at the bottom inlet. The pressure logging frequency is 30 seconds. The outlet has a constant pressure boundary condition. In order to match the time stamp of the logged pressure values exactly to the captured camera images, the pressure time series is synchronized (resampled) to the image series time stamps. One flaw of the current experiment is that air bubbles are present at the top of the tank. However, their effect on the NWP saturation field and the inlet pressure changes should be negligible.

2.4 Data analysis procedure

Two types of drainage images are produced for analyses: 1) NWP saturation maps based on single drainage images and 2) NWP invasion sequence maps by combining multiple drainage images. The NWP invasion sequence map is plotted to show the NWP invasion path throughout the drainage experiment (Glass et al., 2000; Krishnamurthy, 2020). A threshold level of 0.04 is set so that only pixels with NWP saturation increase beyond this threshold compared to the previous time step will be plotted. This is to reduce noise in the resulting plot.

2.4.1 Time series clustering analysis

In this study, we conduct time series clustering in order to correlate changes in the pressure signal to saturation changes in different parts of domain (Ni & Benson, 2020). During the experiment, the saturation field of the entire tank changes through time. This means that each pixel has a saturation value that varies with time, and when plotted against time forms a time series. One useful data analysis tool that assists with analyzing a large quantity of NWP saturation time series data is the clustering algorithm.

Clustering algorithms can group pixels with similar time series behavior together and extract meaningful patterns out of unorganized data. One important metric to define for a clustering algorithm to work is the distance (dissimilarity) between the pixel-wise time series data. In this study, the cosine distance metric is used so that time series with similar trends instead of absolute

values will be grouped together. Two commonly used clustering algorithms exist, K-means and hierarchical clustering methods (James et al., 2013). In this study, due to the large number of pixels present, the K-means clustering algorithm is used because it has a memory advantage over hierarchical clustering (The MathWorks Inc., 2020). Mathematically, K-means clustering partitions data into a pre-specified number of groups K by minimizing the within-cluster variation that is determined by the distance metric. In this particular case, the cosine distance metric as defined in MATLABTM is shown in Equation 1 for the two p-dimensional time series data points (vectors) (The MathWorks Inc., 2006b).

$$d(\mathbf{x}_{i}, \mathbf{x}_{i'}) = 1 - \frac{\mathbf{x}_{i'} \mathbf{x}_{i'}}{\|\mathbf{x}_{i}\| \|\mathbf{x}_{i'}\|}$$
(1)

The objective of K-means clustering is shown in Equation 2,

where $C_1, ..., C_K$ represent the sets of data points in the K clusters, and $|C_k|$ is the number of data points in the kth cluster (James et al., 2013). An iterative algorithm is commonly used to obtain a local minimum for Equation 2.

The clustering algorithm is applied directly on the pixel-wise NWP saturation time series data without any statistical preprocessing or feature extraction steps (Ni & Benson, 2020). After clustering is done, we compute the cluster NWP volume time series by multiplying the cluster mean (arithmetic) NWP saturation by the cluster pore volume. It is feasible to compute NWP volume this way because the domain has a highly homogeneous porosity field such that the pore volume corresponding to each pixel is similar.

The time series clustering analysis is applied not only to the entire domain, but also to the lower capillary barrier region and the upper capillary barrier region separately. Using the NWP invasion sequence map as a pixel mask, it is easy to conduct the time series clustering analysis only on pixels with significant saturation changes during drainage. Increasing the number of clusters always reduces the overall within-cluster variation. However, this comes at a cost of reduced interpretability of what each cluster represents. Therefore, only two clusters are used in each clustering analysis on different parts of the domain so that results are clearly interpretable.

2.4.2 Time series frequency analysis

In order to better analyze how the pressure measurements are related to the saturation field, we can compute linear correlation between the pressure and the cluster volume time series data obtained from the previous clustering analysis. However, because there are often phase shifts between the different time series curves, simple linear correlation may not be able to reflect the true relationships among the data. Therefore, further frequency analysis is conducted. The Fast Fourier Transform algorithm is used to convert the time series signal from the time domain to the frequency domain (Frigo & Johnson, 1997, 1998; The MathWorks Inc., 2006a). The resulting

single-sided amplitude spectrum shows the dominant frequencies, which then yield the true pulsation periods of the time series data (period = 1/frequency).

Because periodic waveforms are necessary for this analysis procedure to yield meaningful results, we apply this frequency analysis procedure to two specific stretches of the time series data where clear periodicity is present, one in the first half of drainage during the regular pulsation period (images 370 to 900), and the other one in the second half of drainage during the stabilized flow period (images 1900 to 2200). The time series data is first detrended (zero-centered) for preprocessing.

2.5 Simulation procedure

The PermediaTM Static Migration module (Halliburton Landmark, 2019) is used to conduct MIP simulations on the beadpack property field. As shown in Figure 1b, the binary domain used for simulation is manually extracted in MATLAB based on the beadpack wet reference image.

The simulator requires as inputs the porosity and the threshold capillary pressure (P_{th}), also known as the capillary entry pressure. Normal distributions for these input parameters are defined for both the coarser-grained matrix and the finer laminae. For porosity, a mean value of 0.4 and the default standard deviation value of 0.01 are used. For P_{th} , the mean values used are specified in Table 2. We then vary the standard deviation P_{th} value from 10 to 100 Pa for the matrix, and keep it at a constant value of 10 Pa for the laminae. The default values for the irreducible water saturation (0.2) and the critical oil saturation (0.02) are used. A voxel size of 2mm × 2mm × 2cm is selected so that it is at the representative elementary volume scale (Trevisan et al., 2017a). Closed boundary conditions are applied to all sides of the domain. All other simulation input parameters are kept the same as the experimental values. NWP is injected with a single point source at the bottom center of the domain. For Monte Carlo probabilistic simulations, a set of 100 property realizations are generated using the previously defined P_{th} and porosity distributions. Then simulation results from these realizations are combined to compute the mean saturation map.

3 Results

3.1 General experimental observations

During drainage, after the NWP is injected into the domain, it first migrates upward in a single finger. After the NWP hits the lower capillary barrier, it then migrates upward along the slope until it reaches the trap area of the barrier. Then, the NWP backfills the trap until the column height of the pool is high enough to eventually break through the capillary barrier. Finally the NWP keeps migrating upward in a single finger until it hits the upper capillary barrier and repeats the previous invasion steps. After NWP percolates the domain, strong flow pulsation is observed as large pulses of NWP are released periodically from the lower capillary barrier trap region into the upper capillary barrier slope region. However, after the establishment of new fingers, pulsation subsides and the flow is much more stabilized for the rest of the drainage experiment.

Figure 2 shows the NWP saturation fields and the NWP invasion sequence maps. We can see from Figure 2a – b that the fingers have the lowest saturation of about 0-0.1, the capillary barrier

pted Artic

slopes have higher saturation of about 0.1-0.2, and finally the pools accumulating in the capillary barrier traps have the highest saturation of 0.2-0.5 during drainage. The higher-than-residual NWP saturation retained underneath the capillary barriers, especially in the pools, is typical of capillary heterogeneity trapping or local capillary trapping during drainage (Gershenzon et al., 2017; Li & Benson, 2015; Saadatpoor et al., 2010; Trevisan et al., 2017a). The observed NWP pool height, which is about 2.5 cm, is close to what is expected for the density contrast and threshold pressure specifics.

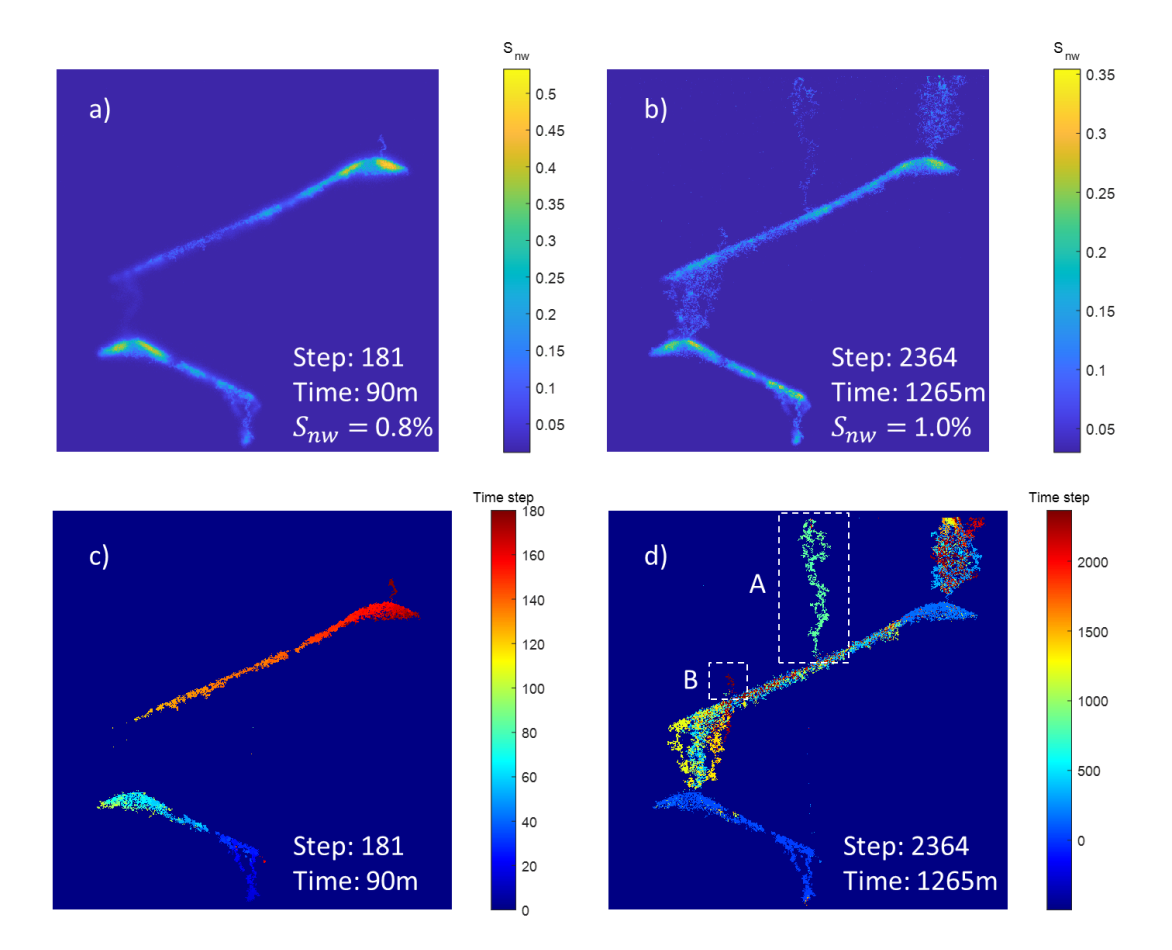


Figure 2. a) NWP saturation field at the time of upper capillary barrier breach. b) NWP saturation field at the end of drainage. c) NWP invasion sequence at the time of upper capillary barrier breach. d) NWP invasion sequence at the end of drainage. White boxes A and B mark two early breaching events through the upper capillary barrier. The time marked shows wall clock time passed in minutes since NWP is first seen in tank. S_{nw} is the domain NWP pore saturation value.

Figure 2c shows that initially the NWP first migrates upslope into the trap of the lower capillary barrier, then keeps migrating upslope into the trap of the upper capillary barrier. However, by the end of drainage as shown in Figure 2d, we can see that there are two distinctly different features from the 2c image. The first one is how the NWP fingers above both of the capillary barrier traps change quite often throughout drainage. The second one is two unexpected early breaching events along the slope of the upper capillary barrier, marked by white boxes. The color of early

breaching event A indicates that some NWP passes through this finger during the middle of drainage before abandoning this flow path again.

3.2 Time series clustering analysis

Figure 3 shows the time series clustering analysis results. From the cluster index maps shown in Figure 3a - c, we can see that when the clustering algorithm is applied to the whole domain, cluster 1 represents the major flow path and cluster 2 represents the fingers. Whereas when the clustering algorithm is applied to just the lower or the upper capillary barrier regions, cluster 1 represents the flow path along the slope and cluster 2 represents the pool in the trap at the top of the capillary barrier.

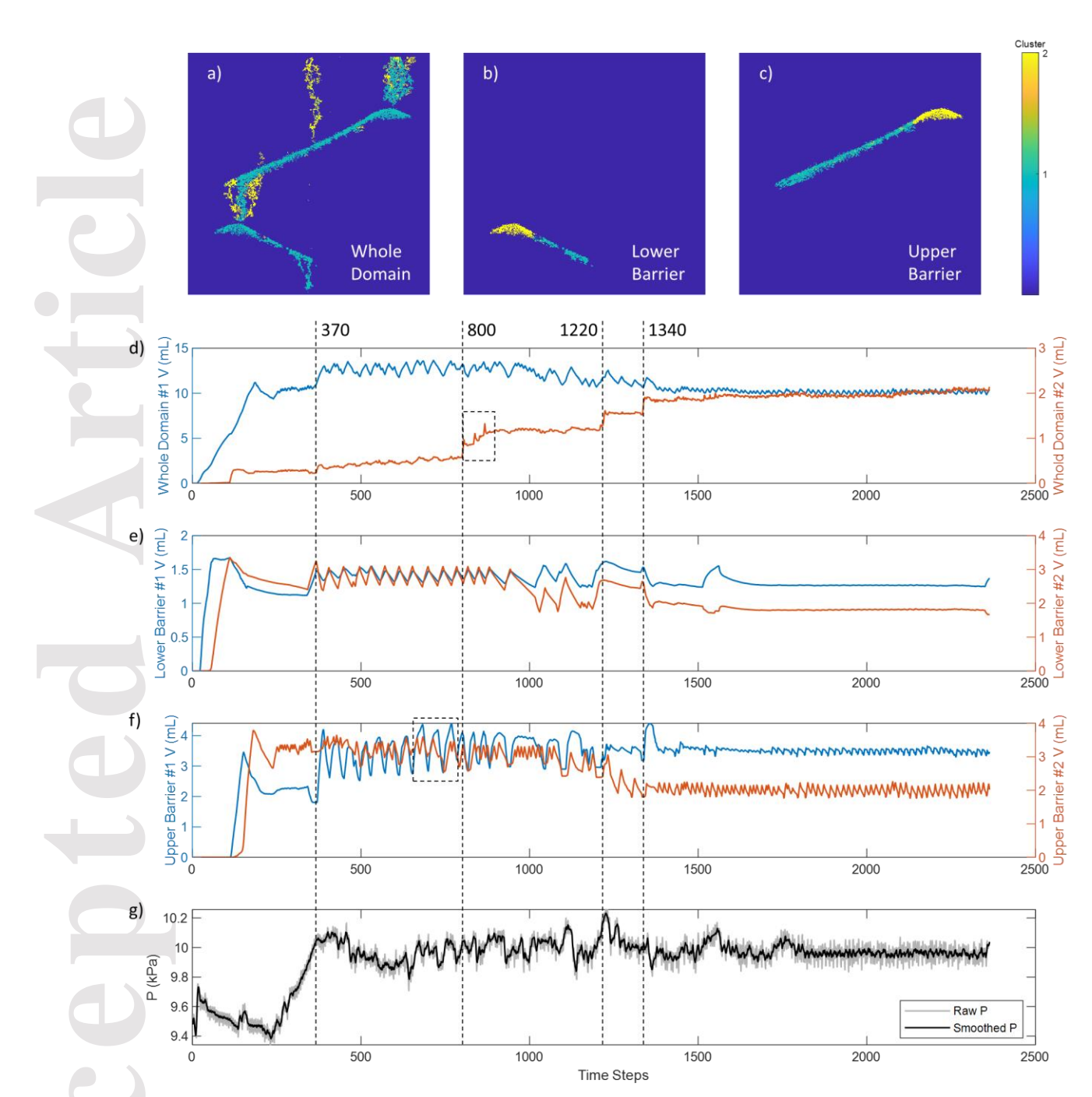


Figure 3. a) -c): K = 2 cluster index maps for the whole domain, just the lower barrier, and just the upper barrier respectively. d) -f): Drainage NWP volume time series for the clusters shown in a) -c). g): Raw and smoothed (span = 5) synchronized inlet pressure response time series. Black dashed lines mark time steps at which significant time series feature changes occur.

Figure 3d – f shows that clear pulsation behavior exists not only in the whole domain but also in each of the capillary barrier regions during the first half of drainage. The NWP overcomes the threshold capillary pressure of the lower capillary barrier by building up column height in the trap region and is released through a finger into the slope region of the upper capillary barrier.

Accepte

This pulsation behavior manifests as triangular waveforms in the various cluster NWP volume time series data. We can see that during the first half of drainage, both the slope and the trap regions behave highly similarly in the lower capillary barrier region in Figure 3e. Whereas for the upper capillary barrier as shown in Figure 3f, the shape of the waves appears quite different. During the second half of drainage, although the flow is much more stabilized, small pulsation behavior can still be seen in the upper capillary barrier region in Figure 3f.

From Figure 3, we can see that there are several time steps at which interesting flow behavior occurs. The corresponding beadpack NWP saturation maps of these time steps are shown in Figure 4. It is clear that at time step 370, the onset of the strong pulsation behavior is caused by the establishment of a new finger flow path between the lower and the upper capillary barriers, as shown in Figure 4a. Next, around time step 800, we can see from Figure 3d that the cluster (#2) representing the finger flow paths has three distinct spikes in its NWP volume time series boxed by black dashed lines. Figure 4d – f shows the first of such spikes, which are caused by the NWP breaching the slope of the upper capillary barrier. The reason for this can be found in the black dashed line box in Figure 3f, where we can see that right before this early breaching occurs at time step 800, there are three large pulses of NWP traversing through the slope of the upper capillary barrier. The NWP volume released in these three pulses is greater than the previous ones as can be seen from the amplitude of the peaks. The raw image sequence of these three pulses clearly shows that with each pulse, the NWP invades more pore space both in the matrix and in the upper capillary barrier itself. Thin fingers can be seen growing in several places in the upper capillary barrier during these three pulses, including locations for both early breaching events A and B as specified in Figure 2d.

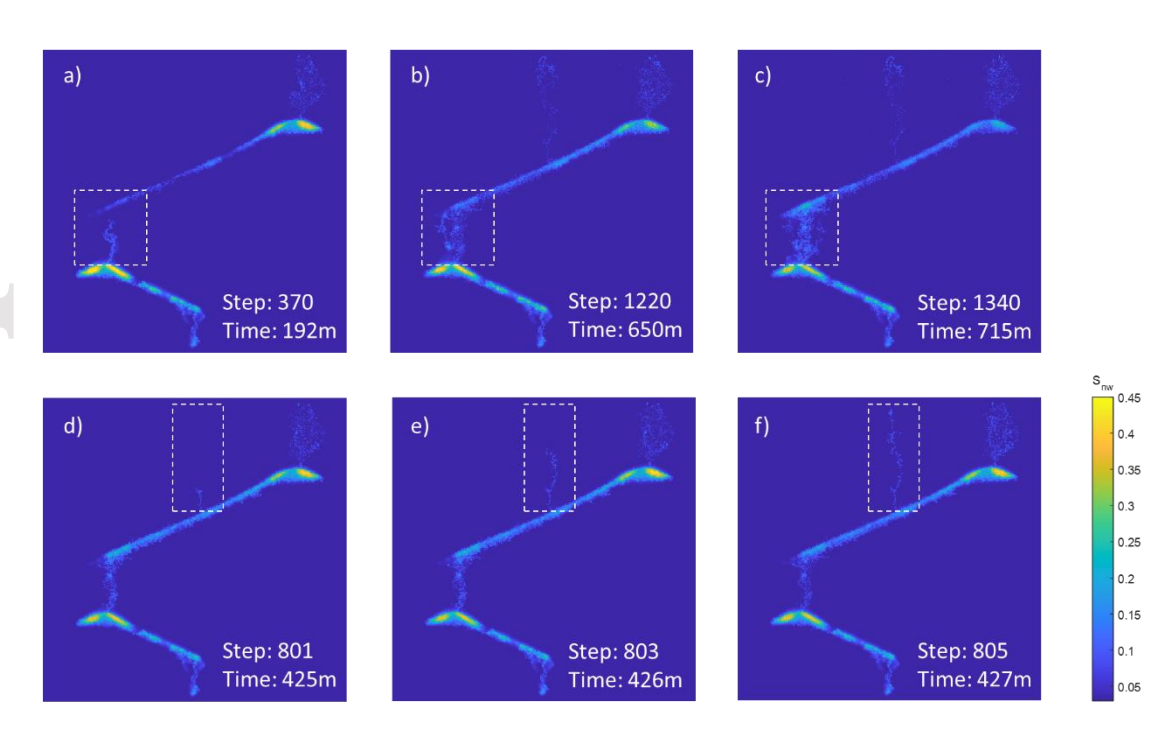


Figure 4. NWP saturation fields at different critical time steps as marked in Figure 3. The time marked shows wall clock time passed in minutes since NWP is first seen in tank. White boxes show regions of interest at the time steps indicated.

After that, at time steps 1220 and 1340, as shown in Figure 3d and Figure 4b – c, the formation of two new finger flow paths in the white boxed region shuts down the strong pulsation behavior and leads to a much more stabilized flow throughout the domain during the second half of drainage. This can also be seen the inlet pressure response in Figure 3g. At the beginning of drainage, because effluent fluid is still filling the outlet reservoir to build up hydrostatic head, true constant pressure boundary conditions at the outlet is not reached until around time step 370. Before time step 1340, the pressure response is highly varying, but after that time step, the pressure response is generally more stable.

3.3 Time series frequency analysis

Figures 5 and 6 show the results of the frequency analysis conducted on two stretches of the time series data. Figure 5 shows the small pulsation behavior that occurs during the stabilized flow period in the later stage of the drainage process. The amplitudes of the NWP volume time series waveforms are small and the pulsation periods are short, only about 500 sec in all of the four regions of the domain as shown in Figure 5a – d. Although the NWP volume time series waveforms all look rather different in the time domain with a relatively low linear correlation with each other, in the frequency domain they have the same dominant frequency.

However, the same pulsation period is not seen in the pressure time domain in Figure 5e. In the frequency domain, much higher frequencies or shorter pulsation periods are observed in the pressure data, which appear to be just noise. The pulsation behavior in fluid flow is so small here that it is probably beyond the detection sensitivity of the pressure transducer. Therefore, in the pressure signal we can only observe noise.

Figure 6 shows the prominent pulsation behavior that occurs during the early stage of the drainage process. The amplitudes of the NWP volume time series waveforms are larger and the pulsation periods are longer, at about 1250 sec in all of the four regions as shown in Figure 6a – d. In the lower barrier region in Figure 6a – b, the NWP volume time series waveforms in the two clusters are exactly in phase and they are both exactly out of phase with the cluster in the upper barrier slope (#1) region in Figure 6c. Therefore, their linear correlations are relatively high. Although no clusters or regions have high correlation with the pressure data.

In Figure 6d, although this upper barrier trap (#2) region also has the same dominant frequency peak at 0.0008 Hz as the other regions, we can observe another three neighboring frequency peaks as marked by the red circles. With these four frequencies combined, the data for this cluster in the time domain appears more erratic than the others. As for the pressure data, from Figure 5e we know that there are high-frequency noise signals present. However in Figure 6e, even with the noise signals still present, the same four low-frequency peaks can be observed in the pressure frequency domain. We apply a lowpass filter to the pressure time series data to get rid of all the higher-frequency noise (The MathWorks Inc., 2018). The resulting lowpass pressure signal shown in the time domain in Figure 6e looks somewhat similar to the NWP volume changes in Figure 6d. This result shows that the pressure response is most closely related to the flow behavior in the upper barrier trap region.



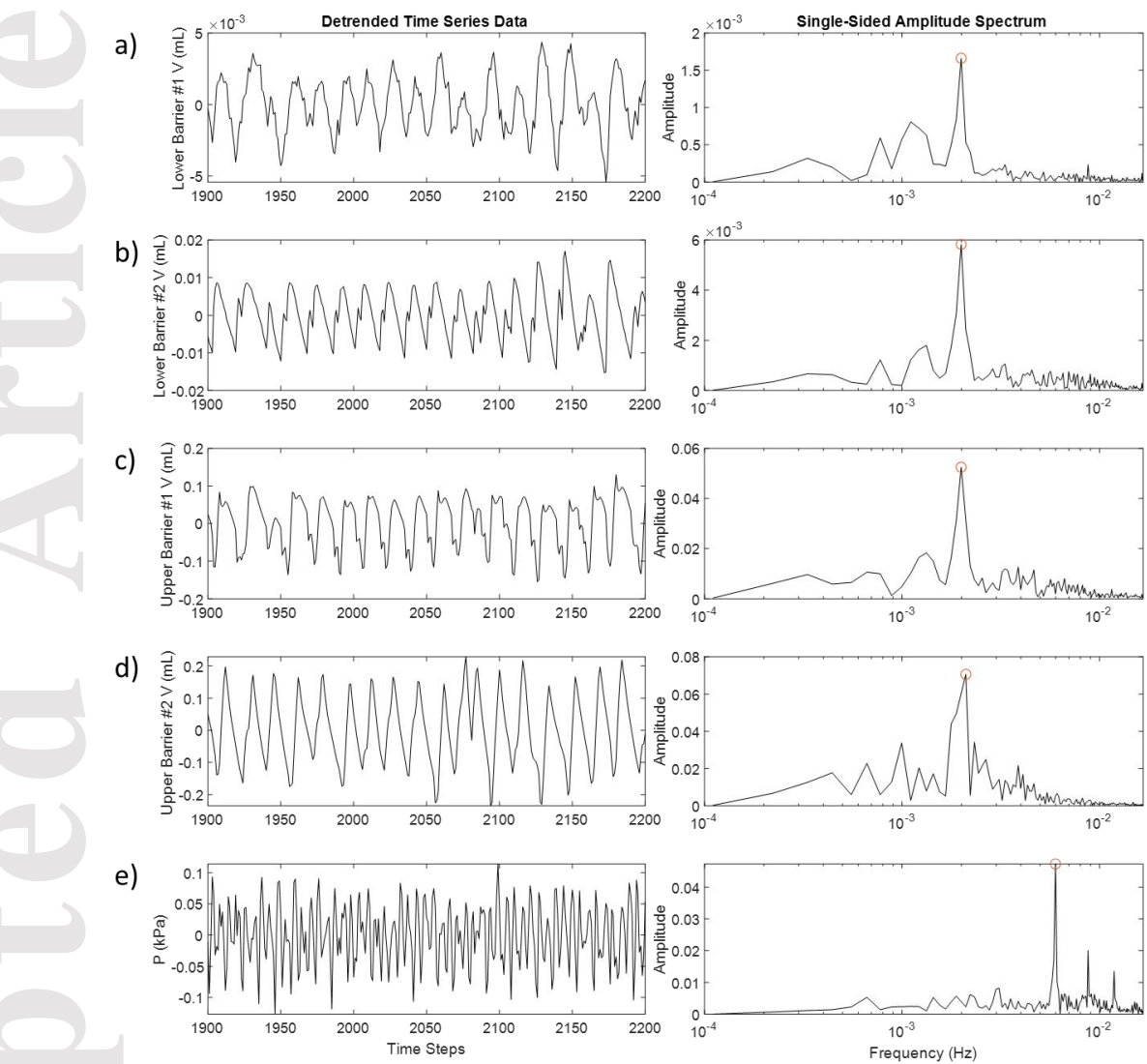


Figure 5. Frequency analysis of the cluster NWP volume time series data between time steps 1900 and 2200. The left hand side shows the detrended time series data in the time domain and the right hand side shows the corresponding data in the frequency domain. Red circles mark the most dominant frequencies. Panels a) and b) correspond to the two clusters shown in Figure 3b and 3e; panels c) and d) correspond to the two clusters shown in Figure 3c and 3f; panel e) corresponds to the inlet pressure shown in Figure 3g.

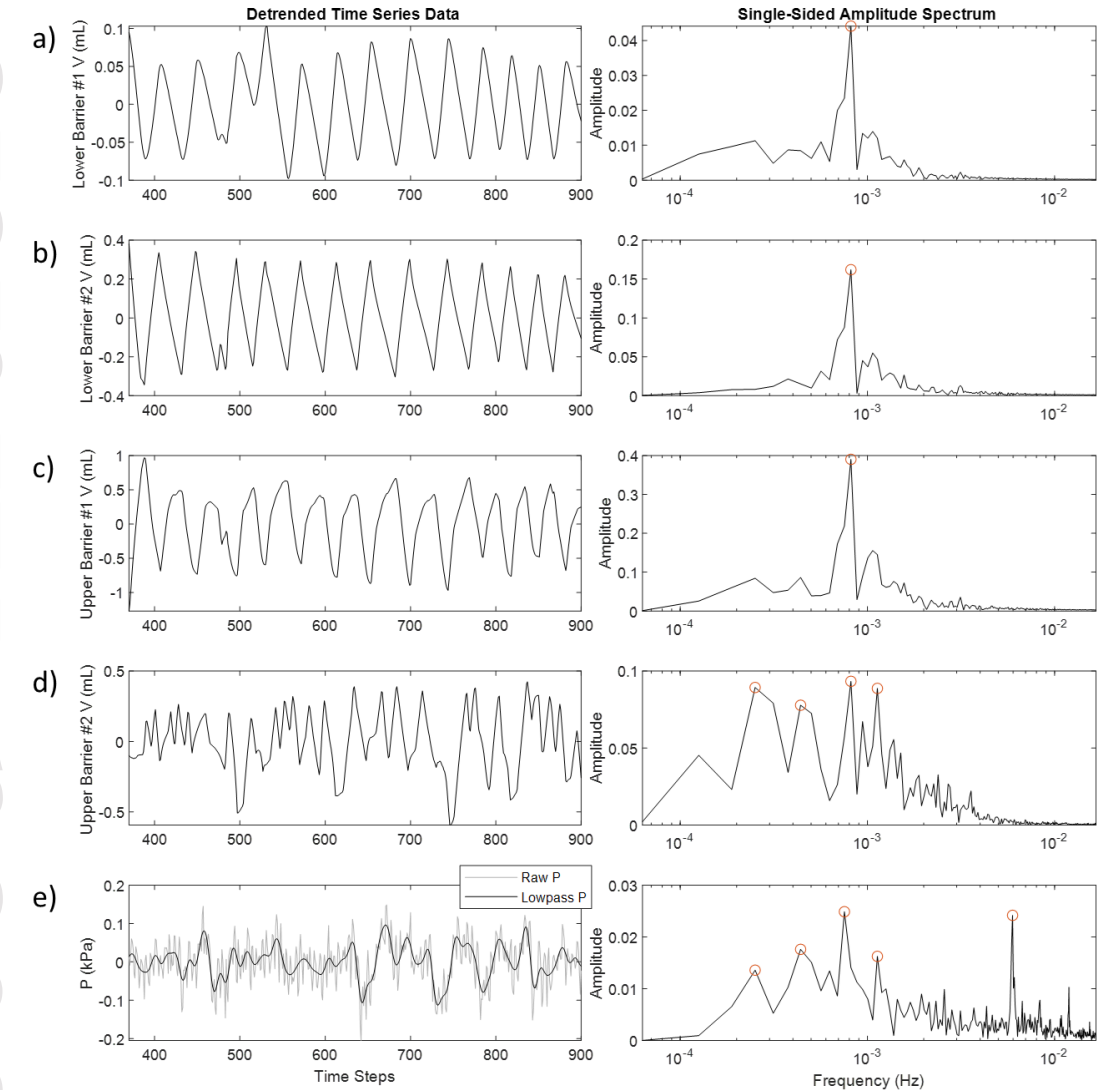


Figure 6. Frequency analysis of the cluster NWP volume time series data between time steps 370 and 900. For more detailed figure description, see Figure 5.

3.4 Comparing simulation and experimental results

The MIP numerical simulation results conducted on the domain shown in Figure 1b are displayed in Figure 7. Figure 7d – f shows three independent simulation runs. The only difference among the three property fields is that the matrix standard deviation P_{th} value as shown in Figure 7a – c. One immediate observation that can be made is that by increasing the matrix standard deviation P_{th} value, one can increase the tortuosity of the NWP flow path, which can cause enough column height to be built underneath the slope region of the upper capillary barrier that NWP will breach early like in Figure 7e. However, when the matrix is extremely heterogeneous and overlaps with the laminae property like in Figure 7c, then the laminae stop

functioning as capillary barriers, as shown in Figure 7f. Furthermore, because the simulation always stops at NWP domain percolation, it is clear that although the backfilling observed in Figure 7d and the early breach along the slope observed in Figure 7e are both present in a single drainage experiment, these two kinds of flow behavior cannot both be simulated in a single MIP simulation run. This is because the Permedia static migration module is not capable of simulating dynamic flow behavior after NWP percolation in a domain. Therefore, no pulsation behavior, establishment of new fingers, or early breaching behavior as seen in experiments can be simulated in a single run.

Another major difference between the single-run simulation results shown in Figure 7a - c and the experimental results shown in Figure 2a - b is the range of NWP saturation values. Although the simulated and the actual overall domain NWP saturation values are similar, the simulator assigns the same default irreducible water saturation to all invaded cells regardless of whether the cell belongs to a finger or a pool, hence giving simulated NWP saturation values that are inconsistent with experimental results.

To address the afore-mentioned inconsistencies, we conduct probabilistic modeling by combining simulation results from many different runs. The results are shown in Figure 7g - i. From the results, we can get a good sense of the range of NWP saturation values, the locations for the fingers, the likely pool height, and finally, whether early breaching is likely to occur. From Figure 7g - i, we can see that when the matrix standard deviation P_{th} value is small, no early breaching through the upper barrier slope ever happens. However, when the matrix standard deviation P_{th} value is larger, there is greater probability that the NWP may breach the capillary barrier slopes before reaching the trap regions. Figure 7g - i also shows the average NWP saturation values across the many different simulation runs. For finger saturation, all simulated values are low and are consistent with experimental values. For pool saturation, while the values are too high in Figure 7g and the pools themselves are nonexistent in Figure 7i, Figure 7i matches most closely with the experimental values. However, in Figure 7h, the saturation of the capillary barrier slope regions is much higher than are seen in the experiment.

Therefore, although the flow saturation and behavior seen in experiments cannot be replicated in a single simulation run, by combining multiple simulation runs, it is possible to replicate at least the probability of the various flow events and the full range of NWP saturation values. By comparing the experimental results with the simulation results, we can conclude that the true matrix standard deviation P_{th} value is likely to be somewhere between 10 Pa and 100 Pa. This is consistent with the standard deviation P_{th} value (~30 Pa) extrapolated based on the known distribution of the matrix glass bead diameters. For computation procedure, see Supporting Information.

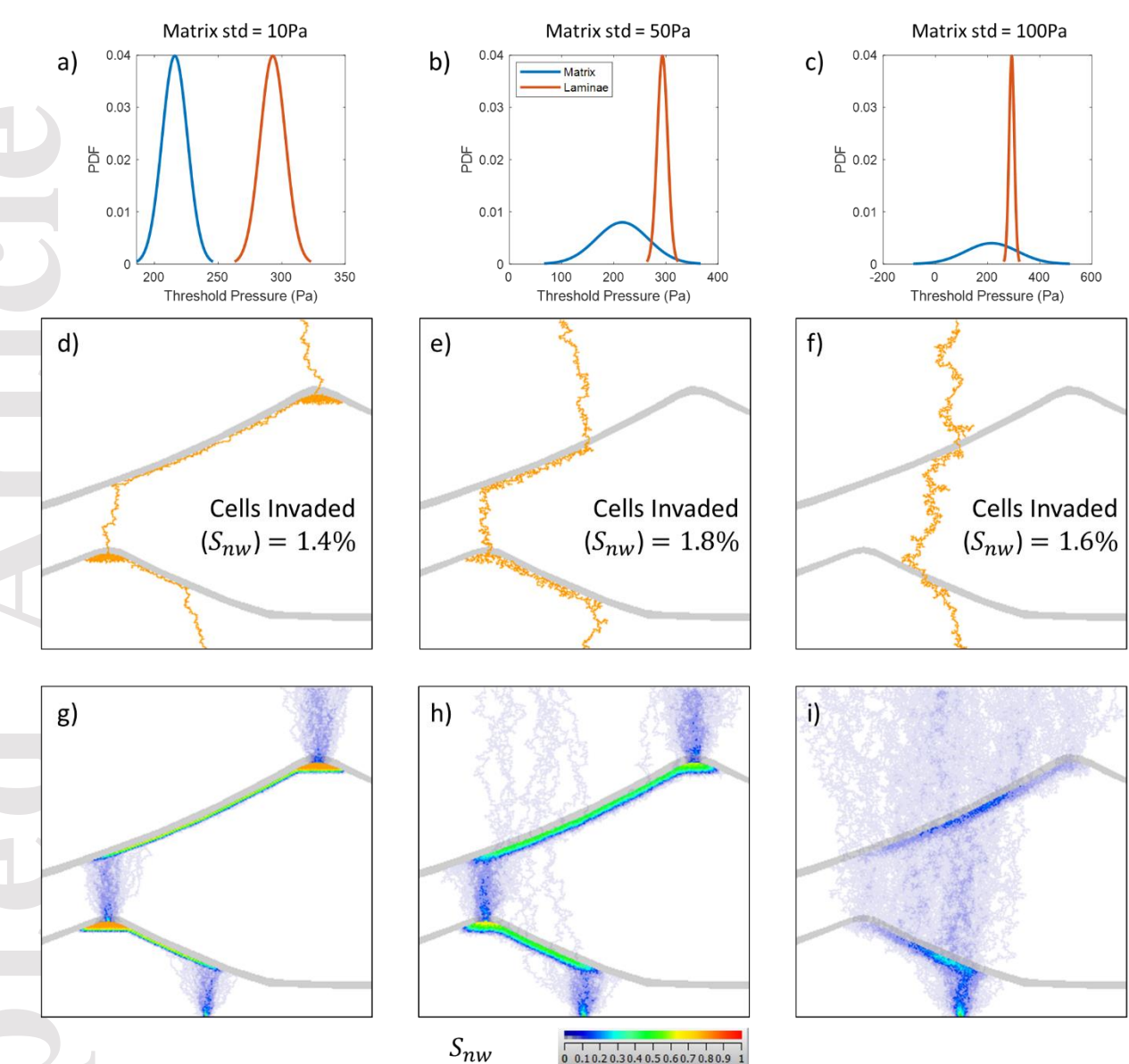


Figure 7. Permedia static migration simulation results. a) -c) Threshold pressure distributions for the matrix and the laminae for the three cases. In all three cases, the laminae standard deviation P_{th} value = 10 Pa. d) -f) Single simulation run on one property field realization. g) -i) Mean S_{nw} maps combining 100 simulation runs on different property field realizations. White: matrix; gray: laminae or capillary barrier.

4 Discussion

The experimental results presented here have shown that even small grain size differences can form effective capillary barriers. Clear NWP flow pulsation and early breaching of the capillary barrier is observed. During the first half of drainage, the strong pulsation behavior also led to observable fluctuations in the NWP inlet pressure. In this section we discuss the reasons behind the pulsation behavior in both the fingers and the pools, how it relates to the capillary pressure, and what the implication of this phenomenon is at the greater scale for CO₂ storage.

4.1 Pulsation in fingers and the pressure response

Many previous micromodel and microCT experiments and simulations have demonstrated that during slow drainage, when gravity forces are negligible, capillary forces dominate, and intermittent NWP flow behavior caused by Haines Jump events is prevalent. A Haines Jump pore invasion event occurs when the NWP front expands into one or more neighboring pores with a sudden burst in the capillary fingering flow regime (Haines, 1930; Tsuji et al., 2016; Zacharoudiou et al., 2018). Consequently, the pore-scale capillary pressure displays sudden reductions that represent such Haines Jump events and therefore show irregular fluctuations in its measurement (Biswas et al., 2018; Furuberg et al., 1996; Måloy et al., 1992; Moebius & Or, 2014; Primkulov et al., 2019; Tsuji et al., 2016; Zacharoudiou et al., 2018).

Interestingly, vertical beadpack experiments have shown that when gravity forces are significant during slow drainage, pore-scale flow behavior is markedly different. Intermittent NWP flow with repeated fragmentation and reconnection events between various isolated macroclusters tend to be the case in homogeneous domains (Birovljev et al., 1995; Islam et al., 2014; Meakin et al., 2000; Stöhr & Khalili, 2006; Wagner et al., 1997). These NWP macroclusters within a finger structure can extend over many pores and have a cm-level length scale (Geistlinger et al., 2006). Capillary pressure first builds up, then when the critical macrocluster height is reached, gravity causes the WP to reinvade critical pores upstream on the backbone of the finger structure (Glass et al., 2000). This leads to NWP macrocluster fragmententation (snap-off), propelling the macrocluster upward under buoyancy, and the pressure instantly drops. Then the process repeats itself as more NWP is supplied upstream and reconnects the isolated macroclusters. Hence we would expect to see more regular pulsation in capillary pressure (Geistlinger et al., 2006; Mumford et al., 2009). However, This is not observed in the inlet pressure response in our experiment. The reasons may be: 1. The heterogeneity in the domain interferes with NWP flow in fingers; 2. Pressure transducer logging frequency is too low.

Glass et al. (2000) have confirmed that the NWP is not continuous in the vertical domain. The fingers appear to have a range of saturation values, indicating that a finger is not one single connected flow path, but rather a series of disconnected macroclusters. This is also apparent because if the finger were a single connected phase then it would build up an enormous column height and breach any capillary barrier immediately instead of migrating beneath it (Meakin et al., 2000). Therefore, the only possible reason for how the inlet pressure transducer can detect NWP pulsation occurring in the far region of the domain is pressure conduction through the WP. This is possible assuming that the WP is incompressible.

NWP flow pulsation in fingers under buoyancy can occur as long as the flow rate is low regardless of grain sizes (Geistlinger et al., 2006). During these slow drainage processes, NWP invasion is steplike because entire old flow paths can be abandoned and trapped after snap-off when entire new pathways are formed (Geistlinger et al., 2006; Stöhr & Khalili, 2006). The same kind of finger formation-and-abadonment behavior is also apparent in our experiment as shown in Figure 3a, d by cluster #2.

4.2 Pulsation in pools

Similar pulsation behavior in NWP pools underneath capillary barriers has also been observed in previous sand-tank experiments conducted by Glass et al. (2000). Their packed sand structure

mimics natural geologic heterogeneity and includes four major capillary barriers. In the authors' CO₂/water experiment, all four capillary barrier regions display pool throbbing/pulsation behavior. By computing the theoretical column height in pools with and without viscous forces, the authors have concluded that viscous forces are negligible when NWP is backfilling in pools underneath capillary barriers. Pool pulsation occurs because as the column height of the pool builds up to some critical value, the NWP breaks through the capillary barrier through a finger. Then as the pool height decreases, the finger flow path cannot be sustained and the WP reinvades the smallest pores in the capillary barrier, fragmenting the finger and closing the flow path. Then the cycle repeats itself as the pool height builds up again (Glass et al., 2000).

Figure 4 in Glass et al. (2000) shows the CO₂ saturation time series data for the four different capillary barrier regions. Although it is unknown as to why the four regions display distinctly different pulsation behavior, the same general trend can still be observed. That is, the lower capillary barrier (CB2) has more regular pulsation than the upper capillary barrier (CB4), just like what we observed in our experiment as shown in the left-hand-side time-domain panels in Figure 6b, d.

During the second half of drainage, it is possible that the small, regular pulsation in the NWP as shown in Figure 5a – d is caused by the pool pulsation mechanism described above. However, another possible explanation is due to the pump used, because peristaltic pumps are known to generate small but noticeable pulsation behavior (Masterflex, 2020).

4.3 Early breaching

Early breaching of the upper capillary barrier at two different locations as shown in Figure 2d can be attributed to three possible reasons: 1. Column height buildup due to a fully connected flow path; 2. Enough viscous forces due to large volumetric pulses of NWP flowing through a limited number of pores; 3. Fracturing of the unconsolidated beadpack due to low overburden pressure (Fauria & Rempel, 2011; Holtzman et al., 2012; Islam et al., 2014).

The main reason behind the early breach at location A in Figure 2d in our experiment is likely to be reason #1. This is because the capillary barrier in question does not require a high capillary pressure to enter. Hence, when just enough NWP volume is present to sustain the critical column height, early breach can occur. However, Glass et al. (2000) uphold reason #2, and they believe that local viscous forces are responsible for the NWP breaching the capillary barrier early instead of flowing underneath and around it. This is likely the reason for early breaching at location B in Figure 2d because the breach location is directly above an actively flowing finger.

Although globally viscous forces are not important because of the low NWP injection rate, locally viscous forces may become as important as capillary forces in the presence of gravity (Glass et al., 2000). To better compare the strength of the local viscous forces versus the buoyancy forces, we compute the respective pressure drop on a connected NWP flow path that is 2 cm tall. This is approximately the height of the NWP flow path along the slope of the capillary barriers. Results indicate that buoyancy forces can be an order of magnitude greater than local viscous forces. Although local viscous forces become more significant as the width of the NWP flow path narrows (Glass et al., 2000), column height buildup is still one of the main reasons for capillary barrier breaching. Therefore, in most cases, Permedia MIP simulations, which ignore

viscous forces, global or local, can still satisfactorily simulate the NWP saturation field even when flow pulsation occurs. The exact calculation procedure can be found in Supporting Information.

Out of the three possible reasons listed, reason #3 is the least probable. This is because if it were true then we should expect the pore structure to be permanently deformed and the conduit to remain open to flow for the remainder of the experiment. Furthermore, points along the capillary barrier above the early breaching point should also display such fracturing behavior because having lower overburden pressure is more susceptible to fracturing (Fauria & Rempel, 2011; Holtzman et al., 2012; Islam et al., 2014).

Note that the experiment has been repeated by manually repacking the tank with similar bead patterns. However, while strong pulsation behavior is observed in repeated experiments at low flow rates (0.02 and 0.2 mL/min), early breaching behavior is not. This is consistent with the Permedia simulation results shown in Figure 7h, as only about 10% of all stochastic runs result in early breaching in the upper barrier. Repeated experiments have also shown that when the flow rate is increased to 2 mL/min, flow is stabilized with no strong pulsation. This is consistent with previous experimental results on the transition flow rate between incoherent and coherent flow regimes for the specific grain size used in our case (Geistlinger et al., 2006).

4.4 Simulations and larger-scale implications

Although Glass et al. (2000) have concluded that the pulsation behavior would not significantly impact large-scale CO₂ flow, the early breaching events observed in our experiment indicate that when occurring at scale this strong pulsation behavior may cause the CO₂ plume to migrate upward through the capillary barriers faster than expected. However, this is only a concern if the formation is relatively homogeneous with sparse capillary barriers. As demonstrated by Krishnamurthy (2020), pulsation behavior is most observable in more homogeneous domains and lower flow rates, but as the grain size difference between the matrix and the laminae increases to produce more capillary barriers, flow pulsation appears to be suppressed.

Therefore, selecting storage formations with dense capillary barriers present is beneficial for suppressing early breaching and retaining more CO_2 as the plume migrates upward under buoyancy. However, interestingly, the simulation results here have shown that having a higher degree of total heterogeneity does not always directly translate to delayed percolation and more CO_2 retention, but the degree of contrast between the matrix and the laminae also matters. This result is consistent with the MIP simulation study conducted by Trevisan et al. (2017a), where the authors have shown that domains with highly heterogeneous but overlaping matrix and laminae threshold properties have much less NWP saturation at the end of drainage than domains with highly homogeneous but non-overlapping matrix and laminae propertity fields (e.g. case 37 vs. case 5 for domain #3). Although the overall degree of heterogeneity of the domains may be similar, the architecture of how the different grain sizes are distributed in the domain plays a vital role in determining the final post-drainage domain NWP saturation retained. Note that although the P_{th} values of real sandstone rocks are much higher than those of the glass beads, because CO_2 retention is caused by relative P_{th} differences between the matrix and the laminae, we would expect similar flow behavior in actual reservoirs.

5 Conclusions

In this study, we conducted a beadpack drainage experiment, analyzed the data, and compared results to numerical flow simulations. Unexpected early breaching events through the upper capillary barrier are observed in the experiment. Analysis has shown that this is likely due to the strong NWP pulsation behavior present during drainage. During drainage, it is observed that the establishment of new finger flow paths both activates and shuts down the strong NWP flow pulsation. Further analysis of the pulsation behavior in the frequency domain has demonstrated that the inlet pressure can respond to saturation changes in regions far away from the inlet, indicating that the WP is the pressure conduit. Finally, MIP simulations were carried out in an attempt to history-match the experimental results. The simulation results have shown that backfilling and early breaching as seen in experiments cannot both be simulated in a single static simulation. However, with Monte Carlo simulation, the probability of these events can be satisfactorily replicated.

Acknowledgement

This material is based upon work supported by the Department of Energy under DOE Award Number DE-FE0031558. The experimental data is available on the Digital Rocks Portal: https://www.digitalrocksportal.org/projects/379. A video of all the drainage images is also provided with the dataset. The authors have no known financial conflicts of interest.

Disclaimer

This report was prepared as an account of work sponsored by an agency of the United States Government. Neither the United States Government nor any agency thereof, nor any of their employees, makes any warranty, express or implied, or assumes any legal liability or responsibility for the accuracy, completeness, or usefulness of any information, apparatus, product, or process disclosed, or represents that its use would not infringe privately owned rights. Reference herein to any specific commercial product, process, or service by trade name, trademark, manufacturer, or otherwise does not necessarily constitute or imply its endorsement, recommendation, or favoring by the United States Government or any agency thereof. The views and opinions of authors expressed herein do not necessarily state or reflect those of the United States Government or any agency thereof.

References

- Birovljev, A., Wagner, G., Meakin, P., Feder, J., & Jøssang, T. (1995). Migration and fragmentation of invasion percolation clusters in two-dimensional porous media. *Physical Review E*, *51*(6), 5911–5915. https://doi.org/10.1103/PhysRevE.51.5911
- Biswas, S., Fantinel, P., Borgman, O., Holtzman, R., & Goehring, L. (2018). Drying and percolation in correlated porous media. *Physical Review Fluids*, *3*(12), 1–11. https://doi.org/10.1103/PhysRevFluids.3.124307
- Bob, M. M., Brooks, M. C., Mravik, S. C., & Wood, A. L. (2008). A modified light transmission visualization method for DNAPL saturation measurements in 2-D models. *Advances in Water Resources*, *31*(5), 727–742. https://doi.org/10.1016/j.advwatres.2008.01.016
- Celia, M. A., Bachu, S., Nordbotten, J. M., & Bandilla, K. W. (2015). Status of CO 2 storage in deep saline aquifers with emphasis on modeling approaches and practical simulations. *Water Resources Research*, *51*(9), 6846–6892. https://doi.org/10.1002/2015WR017609

- Corbett, P. W. M., Ringrose, P. S., Jensen, J. L., & Sorbie, K. S. (1992). Laminated Clastic Reservoirs: The Interplay of Capillary Pressure and Sedimentary Architecture. In *SPE Annual Technical Conference and Exhibition* (pp. 365–376). Society of Petroleum Engineers. https://doi.org/10.2118/24699-MS
- Fauria, K. E., & Rempel, A. W. (2011). Gas invasion into water-saturated, unconsolidated porous media: Implications for gas hydrate reservoirs. *Earth and Planetary Science Letters*, 312(1–2), 188–193. https://doi.org/10.1016/j.epsl.2011.09.042
- Frigo, M., & Johnson, S. G. (1997). FFTW. Retrieved May 2, 2021, from http://www.fftw.org/Frigo, M., & Johnson, S. G. (1998). FFTW: an adaptive software architecture for the FFT. In *Proceedings of the 1998 IEEE International Conference on Acoustics, Speech and Signal Processing, ICASSP '98 (Cat. No.98CH36181)* (Vol. 3, pp. 1381–1384). IEEE. https://doi.org/10.1109/ICASSP.1998.681704
- Furuberg, L., Måløy, K. J., & Feder, J. (1996). Intermittent behavior in slow drainage. *Physical Review E Statistical Physics, Plasmas, Fluids, and Related Interdisciplinary Topics*, *53*(1), 966–977. https://doi.org/10.1103/PhysRevE.53.966
- Geistlinger, H., Krauss, G., Lazik, D., & Luckner, L. (2006). Direct gas injection into saturated glass beads: Transition from incoherent to coherent gas flow pattern. *Water Resources Research*, 42(7), 1–12. https://doi.org/10.1029/2005WR004451
- Gershenzon, N. I., Ritzi, R. W., Dominic, D. F., Mehnert, E., & Okwen, R. T. (2017). Capillary trapping of CO2 in heterogeneous reservoirs during the injection period. *International Journal of Greenhouse Gas Control*, 59, 13–23. https://doi.org/10.1016/j.ijggc.2017.02.002
- Glass, R. J., Conrad, S. H., & Peplinski, W. (2000). Gravity-destabilized nonwetting phase invasion in macroheterogeneous porous media: Experimental observations of invasion dynamics and scale analysis. *Water Resources Research*, *36*(11), 3121–3137. https://doi.org/10.1029/2000WR900152
- Haines, W. B. (1930). Studies in the physical properties of soil. V. The hysteresis effect in capillary properties, and the modes of moisture distribution associated therewith. *The Journal of Agricultural Science*, 20(1), 97–116. https://doi.org/10.1017/S002185960008864X
- Halliburton Landmark. (2019). Permedia. Retrieved from http://www.permedia.ca/
- Holtzman, R., Szulczewski, M. L., & Juanes, R. (2012). Capillary fracturing in granular media. *Physical Review Letters*, 108(26), 1–4. https://doi.org/10.1103/PhysRevLett.108.264504
- Huang, Y., Ringrose, P. S., & Sorbie, K. S. (1995). Capillary Trapping Mechanisms in Water-Wet Laminated Rocks. *SPE Reservoir Engineering*, 10(04), 287–292. https://doi.org/10.2118/28942-PA
- Iglauer, S. (2018). Optimum storage depths for structural CO2 trapping. *International Journal of Greenhouse Gas Control*, 77(July 2017), 82–87. https://doi.org/10.1016/j.ijggc.2018.07.009
- Iglauer, S., Pentland, C. H., & Busch, A. (2015). CO 2 wettability of seal and reservoir rocks and the implications for carbon geo-sequestration. *Water Resources Research*, *51*(1), 729–774. https://doi.org/10.1002/2014WR015553
- IPCC. (2005). IPCC Special Report on Carbon Dioxide Capture and Storage. Prepared by Working Group III of the Intergovernmental Panel on Climate Change. (B. Metz, O. Davidson, H. C. de Coninck, M. Loos, & L. A. Meyer, Eds.), IPCC Special Report on Carbon Dioxide Capture and Storage. Cambridge, United Kingdom and NewYork, NY, USA: Cambridge University Press.
- IPCC. (2014). Climate Change 2014: Mitigation of Climate Change. Contribution of Working

- Group III to the Fifth Assessment Report of the Intergovernmental Panel on Climate Change. (O. Edenhofer, R. Pichs-Madruga, Y. Sokona, E. Farahani, S. Kadner, K. Seyboth, et al., Eds.). Cambridge, United Kingdom and New York, NY, USA: Cambridge University Press.
- Islam, A., Chevalier, S., Ben Salem, I., Bernabe, Y., Juanes, R., & Sassi, M. (2014).

 Characterization of the crossover from capillary invasion to viscous fingering to fracturing during drainage in a vertical 2D porous medium. *International Journal of Multiphase Flow*, 58, 279–291. https://doi.org/10.1016/j.ijmultiphaseflow.2013.10.002
- Jackson, S. J., & Krevor, S. (2020). Small-Scale Capillary Heterogeneity Linked to Rapid Plume Migration During CO2 Storage. *Geophysical Research Letters*, 47(18). https://doi.org/10.1029/2020GL088616
- James, G., Witten, D., Hastie, T., & Tibshirani, R. (2013). *An Introduction to Statistical Learning* (Vol. 103). New York, NY: Springer New York. https://doi.org/10.1007/978-1-4614-7138-7
- Kortekaas, T. (1985). Water/Oil Displacement Characteristics in Crossbedded Reservoir Zones. Society of Petroleum Engineers Journal, 25(06), 917–926. https://doi.org/10.2118/12112-PA
- Krevor, S. C. M., Pini, R., Li, B., & Benson, S. M. (2011). Capillary heterogeneity trapping of CO 2 in a sandstone rock at reservoir conditions. *Geophysical Research Letters*, *38*(15). https://doi.org/10.1029/2011GL048239
- Krishnamurthy, Prasanna G., Meckel, T. A., & DiCarlo, D. (2019). Mimicking Geologic Depositional Fabrics for Multiphase Flow Experiments. *Water Resources Research*, *55*(11), 9623–9638. https://doi.org/10.1029/2019WR025664
- Krishnamurthy, Prasanna Ganesan. (2020). *Geologic Heterogeneity Controls On CO2 Migration and Trapping*. The University of Texas at Austin.
- Li, B., & Benson, S. M. (2015). Influence of small-scale heterogeneity on upward CO2 plume migration in storage aquifers. *Advances in Water Resources*, 83, 389–404. https://doi.org/10.1016/j.advwatres.2015.07.010
- Luo, X., Zhang, F., Miao, S., Wang, W., Huang, Y., Zhou, B., et al. (2004). Experimental verification of oil saturation and losses during secondary migration. *Journal of Petroleum Geology*, 27(3), 241–251. https://doi.org/10.1111/j.1747-5457.2004.tb00057.x
- Måloy, K. J., Furuberg, L., Feder, J., & Jossang, T. (1992). Dynamics of slow drainage in porous media. *Physical Review Letters*, 68(14), 2161–2164. https://doi.org/10.1103/PhysRevLett.68.2161
- Masterflex. (2020). Reducing Pulsation in Peristaltic Pumping Systems. Retrieved from https://www.masterflex.com/tech-article/reducing-pulsation-peristaltic-pumping
- Meakin, P., Wagner, G., Vedvik, A., Amundsen, H., Feder, J., & Jøssang, T. (2000). Invasion percolation and secondary migration: Experiments and simulations. *Marine and Petroleum Geology*, *17*(7), 777–795. https://doi.org/10.1016/S0264-8172(99)00069-0
- Meckel, T. A., Bryant, S. L., & Ravi Ganesh, P. (2015). Characterization and prediction of CO2 saturation resulting from modeling buoyant fluid migration in 2D heterogeneous geologic fabrics. *International Journal of Greenhouse Gas Control*, *34*, 85–96. https://doi.org/10.1016/j.ijggc.2014.12.010
- Moebius, F., & Or, D. (2014). Pore scale dynamics underlying the motion of drainage fronts in porous media. *Water Resources Research*, 50(11), 8441–8457. https://doi.org/10.1002/2014WR015916

- Mumford, K. G., Dickson, S. E., & Smith, J. E. (2009). Slow gas expansion in saturated natural porous media by gas injection and partitioning with non-aqueous phase liquids. *Advances in Water Resources*, 32(1), 29–40. https://doi.org/10.1016/j.advwatres.2008.09.006
- Murphy, W. F., Roberts, J. N., Yale, D., & Winkler, K. W. (1984). Centimeter scale heterogeneities and microstratifaction in sedimentary rocks. *Geophysical Research Letters*, 11(8), 697–700. https://doi.org/10.1029/GL011i008p00697
- Ni, H., & Benson, S. M. (2020). Using Unsupervised Machine Learning to Characterize Capillary Flow and Residual Trapping. *Water Resources Research*, *56*(8). https://doi.org/10.1029/2020WR027473
- Ni, H., Møyner, O., Kurtev, K. D., & Benson, S. M. (2021). Quantifying CO2 capillary heterogeneity trapping through macroscopic percolation simulation. *Advances in Water Resources*, 155(July), 103990. https://doi.org/10.1016/j.advwatres.2021.103990
- Niemet, M. R., & Selker, J. S. (2001). A new method for quantification of liquid saturation in 2D translucent porous media systems using light transmission. *Advances in Water Resources*, 24(6), 651–666. https://doi.org/10.1016/S0309-1708(00)00045-2
- Nordbotten, J. M., Celia, M. A., & Bachu, S. (2005). Injection and storage of CO2 in deep saline aquifers: Analytical solution for CO2 plume evolution during injection. *Transport in Porous Media*, 58(3), 339–360. https://doi.org/10.1007/s11242-004-0670-9
- Primkulov, B. K., Pahlavan, A. A., Fu, X., Zhao, B., MacMinn, C. W., & Juanes, R. (2019). Signatures of fluid-fluid displacement in porous media: Wettability, patterns and pressures. *Journal of Fluid Mechanics*, 875, R4. https://doi.org/10.1017/jfm.2019.554
- Rogelj, J., Shindell, D., Jiang, K., Fifita, S., Forster, P., Ginzburg, V., et al. (2018). Mitigation Pathways Compatible with 1.5°C in the Context of Sustainable Development. In V. Masson-Delmotte, P. Zhai, H.-O. Pörtner, D. Roberts, J. Skea, P. R. Shukla, et al. (Eds.), Global Warming of 1.5°C. An IPCC Special Report on the impacts of global warming of 1.5°C above pre-industrial levels and related global greenhouse gas emission pathways, in the context of strengthening the global response to the threat of climate change, (pp. 93–174). Retrieved from
- https://www.ipcc.ch/site/assets/uploads/sites/2/2019/02/SR15_Chapter2_Low_Res.pdf Rubin, D. M., & Carter, C. L. (1987). *Cross-Bedding, Bedforms, and Paleocurrents*. (L. Crossey & D. McNeill, Eds.) (2nd ed.). SEPM (Society for Sedimentary Geology). https://doi.org/10.2110/csp.87.01
- Saadatpoor, E., Bryant, S. L., & Sepehrnoori, K. (2010). New trapping mechanism in carbon sequestration. *Transport in Porous Media*, 82(1), 3–17. https://doi.org/10.1007/s11242-009-9446-6
- Stöhr, M., & Khalili, A. (2006). Dynamic regimes of buoyancy-affected two-phase flow in unconsolidated porous media. *Physical Review E Statistical, Nonlinear, and Soft Matter Physics*, 73(3), 1–8. https://doi.org/10.1103/PhysRevE.73.036301
- The MathWorks Inc. (2006a). fft. Retrieved May 2, 2021, from https://www.mathworks.com/help/matlab/ref/fft.html
- The MathWorks Inc. (2006b). k-means Clustering. Retrieved February 14, 2019, from https://www.mathworks.com/help/stats/kmeans.html
- The MathWorks Inc. (2018). lowpass. Retrieved May 2, 2021, from https://www.mathworks.com/help/signal/ref/lowpass.html
- The MathWorks Inc. (2020). MATLAB. Natick, Massachusetts: The MathWorks Inc. Retrieved from https://www.mathworks.com/products/matlab.html

- Tidwell, V. C., & Glass, R. J. (1994). X ray and visible light transmission for laboratory measurement of two-dimensional saturation fields in thin-slab systems. *Water Resources Research*, *30*(11), 2873–2882. https://doi.org/10.1029/94WR00953
- Trevisan, L, Krishnamurthy, P. G., & Meckel, T. A. (2017a). Impact of 3D capillary heterogeneity and bedform architecture at the sub-meter scale on CO 2 saturation for buoyant flow in clastic aquifers. *International Journal of Greenhouse Gas Control*, *56*, 237–249. https://doi.org/10.1016/j.ijggc.2016.12.001
- Trevisan, Luca, Pini, R., Cihan, A., Birkholzer, J. T., Zhou, Q., González-Nicolás, A., & Illangasekare, T. H. (2017b). Imaging and quantification of spreading and trapping of carbon dioxide in saline aquifers using meter-scale laboratory experiments. *Water Resources Research*, *53*(1), 485–502. https://doi.org/10.1002/2016WR019749
- Trevisan, Luca, Illangasekare, T. H., & Meckel, T. A. (2017c). Modelling plume behavior through a heterogeneous sand pack using a commercial invasion percolation model. *Geomechanics and Geophysics for Geo-Energy and Geo-Resources*, *3*(3), 327–337. https://doi.org/10.1007/s40948-017-0055-5
- Tsuji, T., Jiang, F., & Christensen, K. T. (2016). Characterization of immiscible fluid displacement processes with various capillary numbers and viscosity ratios in 3D natural sandstone. *Advances in Water Resources*, *95*, 3–15. https://doi.org/10.1016/j.advwatres.2016.03.005
- Wagner, G., Birovljev, A., Meakin, P., Feder, J., & Jøssang, T. (1997). Fragmentation and migration of invasion percolation clusters: Experiments and simulations. *Physical Review E Statistical Physics, Plasmas, Fluids, and Related Interdisciplinary Topics*, 55(6), 7015–7029. https://doi.org/10.1103/PhysRevE.55.7015
- Wilcox, J., Kolosz, B., & Freeman, J. (Eds.). (2021). *Carbon Dioxide Removal Primer*. Retrieved from https://cdrprimer.org/
- Zacharoudiou, I., Boek, E. S., & Crawshaw, J. (2018). The impact of drainage displacement patterns and Haines jumps on CO2 storage efficiency. *Scientific Reports*, 8(1), 15561. https://doi.org/10.1038/s41598-018-33502-y

References from Supporting Information

- Bob, M. M., Brooks, M. C., Mravik, S. C., & Wood, A. L. (2008). A modified light transmission visualization method for DNAPL saturation measurements in 2-D models. Advances in Water Resources, 31(5), 727–742. https://doi.org/10.1016/j.advwatres.2008.01.016
- Glass, R. J., Conrad, S. H., & Peplinski, W. (2000). Gravity-destabilized nonwetting phase invasion in macroheterogeneous porous media: Experimental observations of invasion dynamics and scale analysis. Water Resources Research, 36(11), 3121–3137. https://doi.org/10.1029/2000WR900152
- Hoyt, L. F. (1934). New Table of the Refractive Index of Pure Glycerol at 20° C. Industrial and Engineering Chemistry, 26(3), 329–332. https://doi.org/10.1021/ie50291a023
- Islam, A., Chevalier, S., Ben Salem, I., Bernabe, Y., Juanes, R., & Sassi, M. (2014). Characterization of the crossover from capillary invasion to viscous fingering to fracturing during drainage in a vertical 2D porous medium. International Journal of Multiphase Flow, 58, 279–291. https://doi.org/10.1016/j.ijmultiphaseflow.2013.10.002
- Niemet, M. R., & Selker, J. S. (2001). A new method for quantification of liquid saturation in 2D translucent porous media systems using light transmission. Advances in Water Resources, 24(6), 651–666. https://doi.org/10.1016/S0309-1708(00)00045-2

Potters Industries. (2021). Potters Industries A-Series P-0337 Soda-Lime Silica Technical Quality Solid Glass Spheres. Retrieved August 7, 2021, from http://www.matweb.com/search/datasheet.aspx?matguid=ffdf8138da9f45fb85410873ad90b

Tidwell, V. C., & Glass, R. J. (1994). X ray and visible light transmission for laboratory measurement of two-dimensional saturation fields in thin-slab systems. Water Resources Research, 30(11), 2873–2882. https://doi.org/10.1029/94WR00953

